

Neural Spelling: A Spell-Based BCI System for Language Neural Decoding

Xiaowei Jiang^{1†}, Jinzhao Zhou^{1†}, Yiqun Duan¹, Ziyi Zhao¹, Yu-Cheng Chang¹, Thomas Do¹, Chin-Teng Lin^{*1}

¹Computational Intelligence and Brain Computer Interface Lab, School of Computer Science, Faculty of Engineering and Information Technology, University of Technology Sydney

Abstract—Objective: Brain-computer interfaces (BCIs) can support communication by translating neural activity into text, yet existing non-invasive systems rarely cover the full alphabet, limiting their practical use. **Methods:** We propose a novel non-invasive EEG-based BCI framework, Curriculum-based Neural Spelling (CNS), that decodes all 26 English letters by first learning neural patterns associated with handwriting trajectories. A Generative AI (GenAI) module based on large language models (LLMs) is then integrated to refine spell-based neural decoding and correct semantic errors. **Results:** The proposed system achieves robust letter-level decoding and accurate sentence reconstruction across users, outperforming conventional EEGNet and hybrid CNN-RNN baselines. GenAI correction further reduces word error rates and enhances decoding fluency. **Conclusion:** Combining EEG-based neural spelling with generative language modeling enables full-alphabet decoding and significantly improves linguistic accuracy in non-invasive BCIs. **Significance:** This work demonstrates how integrating GenAI with neural decoding can bridge the gap between noisy signal-level predictions and coherent language-level outputs, establishing a system-level framework for full-alphabet neural spelling and adaptive language-level correction under non-invasive EEG constraints.

Index Terms—Brain-computer interfaces, GenAI, neural language decoding, large language models

I. INTRODUCTION

BRAIN-COMPUTER interfaces (BCIs) have emerged as a pivotal area of research within human-computer interaction (HCI), distinguished by their capacity to seamlessly integrate neural signals with external systems. Pioneering studies such as those by Guo et al.[1], Chen et al.[2], Cao et al.[3], Nguyen et al.[4], and Lin et al.[5] underscore BCIs' role in advancing neuroscience and technology. These interfaces create direct communication pathways that are especially beneficial for individuals with limited speech or motor functions. Language decoding represents a critical domain within BCI research, aimed at deciphering the neural correlates of speech and language processing. This capability not only enhances interaction paradigms but also opens new avenues for communication, offering significant improvements in quality of life for those with severe communicative impairments.

Initially, BCI research focused on visual-based decoding approaches, such as steady-state visually evoked potentials (SSVEP)[1], which, despite their reliability, demand high cognitive effort and are unsuitable for prolonged use[2]. These

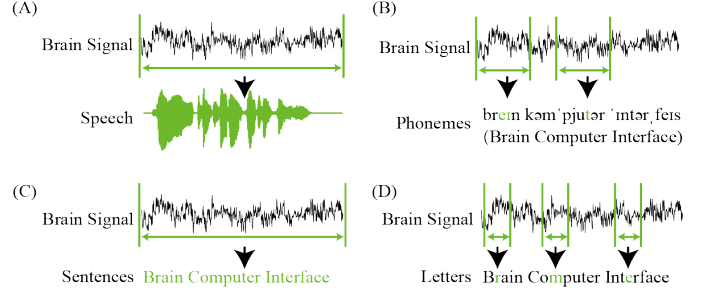


Fig. 1. Demonstrations of **four** typical language decoding frameworks. (A) Direct speech synthesis approach. (B) Spelling-based approach using phonemes. (C) Direct text synthesis approach. (D) Spelling-based approach using letters.

methods often fail to align with natural human language patterns, posing significant usability challenges. The advent of invasive neural decoding technologies marked a significant advancement, allowing for direct interpretation of brain signals via electrocorticography (ECoG) or stereo-EEG (sEEG)[6, 7]. These methods have demonstrated substantial improvements in user performance, significantly enhancing communicative capacities for patients with speech impairments. However, the invasive nature, high cost, and ethical concerns limit their general applicability[8]. In contrast, non-invasive BCIs, predominantly utilizing electroencephalography (EEG), offer a more accessible alternative. These systems are less obtrusive and more cost-effective, broadening potential user demographics [9, 10]. Despite the challenges of signal noise and the extensive training required for users, recent studies have demonstrated EEG's potential in effective language decoding [11, 12].

With the rise of Generative AI (GenAI), the integration of large language models (LLMs) into BCI research has opened new avenues for enhancing language decoding [13]. This integration can be implemented within two distinct frameworks: directly synthesizing speech or text from brain signals using pre-trained LLMs, as illustrated in Fig. 1(A) and Fig. 1(C) respectively; and decoding brain signals into minimal language units such as phonemes, as shown in Fig. 1(B), or letters, as depicted in Fig. 1(D), followed by text generation through natural language processing (NLP) models.

The first framework often faces limitations due to the disparity in data scales between brain data and text/image datasets, which can restrict the system to operating within predefined datasets, merely retrieving sentences rather than

[†]Xiaowei Jiang and Jinzhao Zhou contributed equally to this work.

^{*}Corresponding author: Xiaowei Jiang. Email: xiaowei.jiang-1@student.uts.edu.au

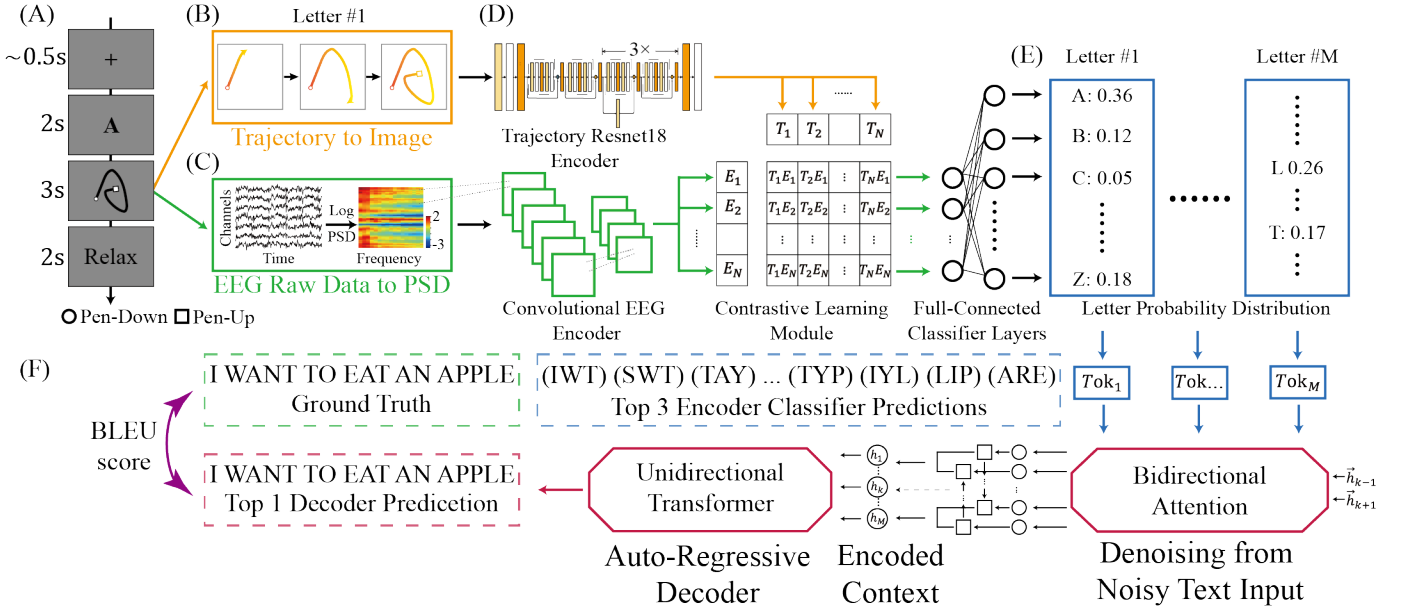


Fig. 2. (A): The experimental design. (B): The trajectory completion over time. (C): The power spectral density (PSD) features computed from raw EEG signals. (D): The structures of the Trajectory ResNet-18 encoder and the Convolutional EEG encoder. (E): The letter probability distribution at the classifier output. (F): The structure of the sentence generator.

generating novel content. The second approach, known as the spell-based method [14, 15], operates by initially decoding neural signals into their minimal representational units, such as the 26 letters, or even nine-key input (T9) [16]. It subsequently employs GenAI to construct coherent text in a second stage. This technique is advantageous as it requires fewer categories for the neural decoding model, thereby reducing both the cognitive load on the user and the difficulty associated with model training. A significant benefit of this method is its utilization of extensive textual datasets in training GenAI, particularly for generative error correction (GEC) [17], which enhances the accuracy and flexibility of the generated text. Moreover, this method is not constrained by the size of the neural training samples and can adapt swiftly to new linguistic content through fine-tuning of the GenAI, circumventing the need for extensive retraining on new brain data.

The spell-based methods initially utilize N-gram models to calculate the probability of sequential letter occurrences. For instance, the ECoG study aimed at spelling imaged handwritten letters [15], and the sEEG study focused on spelling the Pinyin representations of Chinese pronunciations [18]. Subsequently, GenAI technologies have been employed to enhance performance, as demonstrated in studies like [8] and [13]. These vocal-based methods underscore the potential of GenAI for neural language decoding. However, these approaches have limitations. For example, vocal-based methods require accurate pronunciation by subjects. Given the diversity in pronunciation—such as the thousands of syllables and 44 phonemes in English, including closely related sounds like /a/ and /ae/, along with variations between short and long vowels—it becomes challenging to accurately generate complete sentences. Simultaneously, Mandarin Chinese combines 21 consonant phonemes, 7 vowel phonemes, and 4 tones to create over 400

distinct syllables [18]. This vast array of phonetic elements significantly complicates speech synthesis in both languages. The complexity is further exacerbated in non-invasive speech synthesis applications due to the signal-to-noise ratio (SNR) and the limitations of the training datasets available. These factors together pose substantial challenges in developing robust and accurate speech synthesis systems. Therefore, spelling letters, as opposed to using vocal-based features, presents a more effective option for language decoding. The classification of just 26 letters not only simplifies the process compared to pronunciation-based methods but also enhances performance and applicability, even facilitating cross-linguistic utility, such as seamlessly integrating English and Pinyin. Unlike prior EEG-based handwriting paradigms that typically focus on limited symbol sets or isolated character recognition, the present study systematically investigates full-alphabet (26-letter) decoding and further integrates curriculum-adapted language modeling to enable sentence-level reconstruction. To optimize letter input, innovative scenarios have been designed, such as ‘air-writing’ [19] and ‘paper-writing’ [20].

Moreover, cVEP-based systems have demonstrated efficient and reliable performance under non-invasive EEG settings [21], and online P300 spellers have been established as practical communication systems since the seminal work of Farwell and Donchin [22]. More recently, complete sentence-level online spelling pipelines with calibration procedures and large language model integration have also been reported [23]. These approaches represent well-established non-invasive BCI paradigms.

However, a common characteristic of these systems is that they are predominantly *stimulus-driven* or *reactive* in nature, relying on externally evoked neural responses (e.g., visual flickers or oddball paradigms) and predefined symbol sets.

While such paradigms achieve high information transfer rates and robust online performance, they are primarily designed to optimize communication efficiency, but this comes at the cost of increased visual fatigue.

In contrast, handwriting-based BCIs aim to decode *active*, self-initiated motor-related neural activity associated with voluntary letter production, enabling more naturalistic and flexible letter generation without reliance on continuous external stimulation. Despite extensive research on non-invasive spellers, whether an active, handwriting-based BCI can reliably decode the full alphabet (26 letters) from scalp EEG, and thereby establish a normative neural reference for neural handwriting under realistic non-invasive constraints, remains an underexplored problem. The present work addresses this gap by focusing on neural handwriting as an active input paradigm, rather than on stimulus-driven letter selection or communication throughput alone.

This paper contributes to the evolving landscape of brain-computer interfaces (BCIs) by proposing a hybrid approach that merges the accessibility of non-invasive EEG with the advanced linguistic capabilities of GenAI. We introduce a novel curriculum-based neural spelling framework (CNS) for neural language decoding. This framework employs a convolutional neural network (CNN)-based encoder to initially learn individual-specific letter transition patterns, followed by a curriculum-driven LLM to synthesize sentence texts. The results demonstrate significant enhancements in the performance of language decoding tasks. By integrating these advanced technologies, we establish a normative neural baseline for non-invasive neural handwriting under realistic EEG constraints. We aim to facilitate a system-level investigation of full-alphabet neural spelling, demonstrating how low-SNR EEG decoding can be coupled with curriculum-adapted generative language models to enable language-level error correction, heralding a new era in assistive communication technologies. This introduction outlines the transformation of BCI technology from basic visual decoding to sophisticated language synthesis, setting the stage for a detailed discussion on how current technologies can be integrated and enhanced to better meet the communicative needs of a diverse user population.

The contributions of this work are threefold:

- This study is the first to collect and analyze brain dynamics patterns related to EEG-based handwriting of all 26 letters.
- We employ a CNN-based model for EEG encoding, which achieves exemplary top-k accuracy, averaging across all subjects.
- We propose a novel curriculum supervised fine-tuning method that enables an LLM to learn subject-specific letter transition patterns effectively, thereby enabling high-quality sentence synthesis. This approach has shown promising results, achieving high scores on established metrics.

II. RELATED WORK

A. Language Decoding

Recent advances in Language Neural Decoding have significantly enhanced BCI systems. RNN-based models have

achieved a 23.8% word error rate on a 125,000-word vocabulary using chronic ECoG signals, highlighting their potential as speech neuroprostheses [8]. ECoG-based Speech BCIs have demonstrated stable control of assistive devices for up to three months with minimal calibration, supporting daily unassisted use [24]. Additionally, speech synthesis from ECoG signals enables decoding spoken sentences [6], while contrastive learning models have decoded perceived speech from non-invasive recordings like EEG and MEG, enriching decoding techniques [11]. To better predict the text, a novel task, named Cross-Modal Cloze (CMC) task [25], which is to predict the target word with a context as prompt, are proposed, achieving 28.91% accuracy.

Spelling-based BCIs have also progressed, with high-speed systems like the JFPM-based SSVEP speller [14] and NeuroAiR, which uses ICA and EEGNet to achieve 44.04% accuracy in recognizing airwritten letters [19]. Efforts in tonal language decoding and synthesis [26], handwriting tasks [15], and CNN-based classifiers for letter decoding, such as “HELLO, WORLD!” [20], further highlight BCI versatility.

ECoG systems have provided communication solutions for late-stage ALS patients by decoding English letters [27], while silent spelling mechanisms predict characters in 2.5 seconds, improving practical use [28]. CNNs have decoded sentences [29] and simple commands [30, 31], while EEG-based user authentication systems using dynamic signatures have been explored for security [32, 33].

B. Enhancing Text-to-Text Error Correction with Large Language Models

Advances in NLP have been fueled by the emergence of LLMs, which represent a paradigm shift from traditional supervised learning to pretrained models that leverage vast corpora, subsequently fine-tuned or prompted for specific tasks [34, 35]. These models, primarily encompassing BERT-based architectures with bi-directional attention mechanisms [36] and GPT-based models utilizing auto-regressive learning schemas [37, 38], excel at building contextual representations and deriving nuanced understanding from extensive natural language data. As a result, complex language tasks such as document-level translation [39, 40] and advanced question answering [41] can now be performed with minimal supervision.

When it comes to GEC area, LLMs excel at text manipulation tasks such as grammar correction [42], text rewriting [43], and improving spoken language comprehension [44, 45]. By integrating generation and re-ranking, LLMs provide dynamic solutions for error correction and text refinement [46, 47]. Models like ChatGPT [48] and ChatGLM [49] expand these capabilities further, performing text understanding, generation, and correction in unified frameworks. Despite their computational demands, smaller models like BART [50] and T5 [51] offer resource-efficient alternatives for specialized tasks, maintaining robust performance in constrained environments [52].

By integrating LLM-based generative error correction, we can re-organize the slightly disordered output sequence of the neural spelling system into a more fluent language. This improves the overall system performance.

III. PRELIMINARIES

In this section, we introduce the foundational concepts and notation used to describe our two-step neural processing system for EEG-based sentence generation. The system consists of two sequential modules: an encoder for EEG signal processing and a GenAI model to synthesize sentences.

A. EEG Signal Encoder

Let $\mathbf{X} \in \mathbb{R}^{T \times C}$ represent the EEG input where T denotes the number of time steps and C the number of channels. The encoder function, denoted as f_{enc} , transforms \mathbf{X} into a probability vector $\mathbf{p} \in \mathbb{R}^{26}$, with each component p_i of \mathbf{p} representing the probability of the corresponding letter i from the English alphabet:

$$\mathbf{p} = f_{\text{enc}}(\mathbf{X}; \theta_{\text{enc}}) \quad (1)$$

where θ_{enc} are the parameters of the encoder. The encoder utilizes a neural network architecture optimized for temporal and spatial features inherent in EEG data.

B. GenAI Model for Synthesizing Sentences

Upon generating the letter probabilities \mathbf{p} , these are inputted into a GenAI model, g_{trans} , which outputs a coherent sentence \mathbf{y} . This model is based on a pretrained LLM that has been fine-tuned for the task of converting sequences of letter probabilities into grammatically correct and contextually relevant sentences:

$$\mathbf{y} = g_{\text{trans}}(\mathbf{p}; \theta_{\text{trans}}) \quad (2)$$

where θ_{trans} represents the parameters of the translation model. The model leverages advanced natural language processing techniques to ensure semantic coherence and syntactic accuracy in the generated sentences.

These components are integrated to form a robust system for interpreting EEG signals and producing textual outputs, aiming to bridge the gap between neural activities and language expression.

IV. METHODOLOGY

A. Curriculum-based Neural Spelling Framework

This section introduces the Curriculum-based Neural Spelling (CNS) Framework, a novel approach to enhancing the spelling accuracy from neural signals using a two-stage model. Initially, the model utilizes a Convolutional EEG Encoder to transform raw EEG data into a letter classification schema employing minimal neural samples and a tailored set of character categories. In the second stage, we integrate Curriculum Learning with large language models (LLMs) within a sequence-to-sequence framework to generate fluent sentences despite inherent noise and variability in EEG signals. This combination aims to leverage the strengths of advanced neural network architectures and sophisticated natural language processing techniques to overcome the challenges posed by low signal-to-noise ratios and the complex nature of EEG-based letter decoding. The architecture and its components are depicted in Fig. 2, and this comprehensive setup promises significant advancements in brain-to-text communication technologies.

1) Stage 1: Neural Letter Classifier:

a) *Convolutional EEG Encoder:* The Convolutional EEG Encoder is designed as a two-layer Convolutional Neural Network (CNN), which is adept at processing EEG data for the purpose of embedding generation, as shown in Fig. 2D. This encoder operates in conjunction with contrastive learning (ConL) techniques to enhance the discriminative power of the embeddings. The trajectory data is processed by a pre-trained ResNet18 [53] model, which serves as a trajectory encoder. The core of our learning strategy is based on minimizing the contrastive learning loss ($loss_{ConL}$), which is calculated as follows:

The loss function is defined as:

$$loss_{ConL} = 1 - \cos(\theta_{EEG}, \theta_{Traj})^2 \quad (3)$$

where θ_{EEG} and θ_{Traj} represent the embedding vectors from EEG data and trajectory data, respectively.

b) *Classification Head:* The letter classification component is an integral part of the CNS Framework. It includes a fully connected linear layer that maps its input to a 26-node output layer, where each node represents a letter of the English alphabet. After this. This arrangement enables the system to predict letters based on the processed EEG data. A softmax function is applied to the output layer to obtain a probability distribution over the alphabet, as shown in Fig. 2E, which is critical for the system's accuracy in spelling prediction. The classifier utilizes the cross-entropy loss to measure the discrepancy between the predicted probabilities and the actual distribution of the target letters. The crossentropy loss ($loss_{CE}$) function is defined as follows:

$$loss_{CE} = - \sum_{c=1}^M y_{o,c} \log(p_{o,c}) \quad (4)$$

where M is the number of classes (letters), $y_{o,c}$ is a binary indicator (0 or 1) if class label c is the correct classification for observation o , and $p_{o,c}$ is the predicted probability of observation o being of class c . This loss function effectively guides the learning process by penalizing deviations from the true label distribution, thus enhancing the system's ability to generate accurate and reliable spelling predictions from EEG signals.

In the training phase, the final loss ($loss_{total}$) is computed as a weighted combination of the cross-entropy loss ($loss_{CE}$) and the contrastive loss ($loss_{ConL}$):

$$loss_{total} = 0.35 \times loss_{CE} + 0.65 \times loss_{ConL}. \quad (5)$$

The weighting coefficients are selected empirically to balance classification accuracy and representation regularization.

2) *Stage 2: Curriculum Learning for Language Model Integration in Fluent Sentence Generation:* The inherently low SNR of EEG signals combined with the rigorous demands of experimental protocols exacerbates the challenges of prediction biases and data scarcity in letter-level classification. These limitations significantly impede the capacity of classifiers to decode fluent sentences. To mitigate these challenges, we propose the integration of LLMs within a sequence-to-sequence

TABLE I
CHALLENGES IN LETTER-LEVEL NOISE DENOISING WITH CHATGPT 4

Ground Truth: This civilization, known as the 'Ayar,' possesses an advanced understanding of nature and the power to manipulate the very fabric of reality.
Prompt: You are an expert on letter denoising of sentences. The letters from the following sentence are corrupted with noise. Can you guess and output the correct sentence? {decoder_output}
Input: tvmg jifzfmhiog wnewn ms tve awmt pesowogeo in iqeanjqv onzerstmvgvmng oz nmmxrw mgz txw peeer to mmgipxfamw mxe eefw zavfij ov feifatw
Prediction: Time is the most precious thing in life, understanding it makes the effort to simplify the world of survival or benefit.

(seq2seq) framework aimed at enhancing sentence fluency and readability.

Traditional NLP models often struggle with inputs characterized by significant letter-level noise due to their reliance on sub-word-level tokenization and training predominantly on well-curated texts. As depicted in Table I, without a nuanced understanding of the behaviors specific to subject-based letter classifiers, models like ChatGPT4 can generate sentences that diverge significantly from the intended content, typically relying on generalized knowledge of language structure and common phrases.

a) Curriculum Learning Approach: To address these constraints, we introduce a curriculum learning strategy tailored for pretrained LLMs. This strategy is designed to adapt the models to the latent distributions specific to subject-based handwriting patterns. By progressively increasing the relevance to the domain and the complexity of the tasks during training, our curriculum learning approach methodically fine-tunes LLMs. This targeted training enables the models to achieve better alignment with the idiosyncratic characteristics of subject-specific letter decoders, thereby enhancing their capacity to handle noisy inputs and improving overall sentence generation:

- 1) **Initial Phase:** Start with tasks involving high-frequency, low-noise samples to establish baseline language structures.
- 2) **Intermediate Phase:** Gradually introduce more complex and noisier data, increasing exposure to real-world variability.
- 3) **Advanced Phase:** Focus on fine-tuning with the highest noise levels and the most challenging samples to ensure robustness and fluency under the most adverse conditions.

This structured approach not only streamlines the adaptation process but also significantly boosts the model's ability to generalize from noisy, imperfect inputs to coherent and contextually accurate text outputs.

b) Probabilistic Character Sampling from the Neural Letter Classifiers: To evaluate the efficacy of our curriculum-based LLMs, we analyze the letter category distributions, $C_{i,\omega}$, for letter ω in sample i . These distributions are obtained from the softmax-normalized outputs of the classification head. We compute the aggregate Top- K distributions, C_{ω}^* , as follows:

$$C_{\omega}^* = \frac{\sum_{i=1}^N C_{i,\omega}}{N_{\omega}} \quad (6)$$

where N_{ω} denotes the count of samples for letter ω . From this, the letter ω is then probabilistically sampled based on its presence within the Top- K distribution. For instance, consider the ground truth (GT) sentence, "As he chases down rogue time travelers...". If the aggregated probability for 'A' at the start, C_A^* , is 0.2 and for 'R', C_R^* , is 0.6, the classifier might predict "Rs" in place of "As".

c) Implementation of Noise Adaptation: Noise adaptation refers to the process of fine-tuning the language model on EEG decoder outputs that contain systematic letter-level errors, enabling the model to recognize and correct typical noise patterns arising from neural decoding during inference. In this phase, we incorporate the noisy predictions from the Neural Letter Classifier (NLC) into the LLM's training regimen. Specifically, we replace selected characters in the training texts with their corresponding noisy variants from the Top- K output distributions. The LLM is then fine-tuned to de-noise this altered text. This structured noise adaptation process is designed to enhance the model's robustness, enabling it to effectively manage and correct noisy inputs during inference.

d) Curriculum Arrangement: In our curriculum learning method, training examples \mathbf{D} are arranged according to a complexity score \mathbf{C} , in a multi-stage setting $\{T_i : i = 1, 2, \dots, N\}$. In each stage T_i , a percentage $c \in \mathbf{C}$ of the letters from the input sentences will be permuted by the letter prediction distribution of the letter-classifier model, with a linear increase in the complexity score c .

e) Supervised Fine-tuning: We employ bi-directional attention during training for this seq2seq generation task, as shown in Fig. 2(F). The fine-tuning objective combines the denoising training objective with the causal language modeling objective [50], facilitating the model's use of previously generated tokens to guide the prediction of subsequent tokens, thereby reducing the influence of noisy letter-level inputs.

$$\mathcal{L}_{LMft} = - \sum_{t=1}^T \log P(y_t | \mathbf{x}, y_{<t}) \quad (7)$$

where $y_{<t}$ represents the previously generated tokens, and \mathbf{x} is the noisy input sentence. In the subsequent Section V-F, we will explore the performance benefits of the fine-tuned LLMs pretrained model utilizing our curriculum learning method in comparison to direct and non-fine-tuning approaches. Additionally, we will examine how variations in model size influence performance metrics.

The sensitivity analyses of the proposed curriculum learning (CL) strategy with respect to two key factors, noise injection strength and the number of curriculum stages, as well as the influence of different curriculum schedule shapes on model performance, are presented in Supplemental Sections I.A and I.B.

V. EXPERIMENTS AND RESULTS

A. Participants

We recruited thirty-two right-handed, healthy individuals (P1–P32), all native English speakers from Australia, comprising 16 males and 16 females with an average age of $M_{\text{age}} = 24.94 \pm 0.29$ years. Each participant had normal or

corrected-to-normal vision and reported no history of mental health disorders. Four subjects were removed from the dataset due to misunderstanding of the experimental instructions. An a priori power analysis (G*Power v3.1.9.7) indicated that approximately 30 participants are sufficient to detect medium within-subject effects (Cohen’s $d_z = 0.5$) at a significance level of $\alpha = 0.05$. The final sample size therefore meets standard statistical power requirements for within-subject EEG analyses. Ethical approval was granted by the University of Technology Sydney’s Ethics Committee (Approval No. UTS HREC REF: ETH23-8036). Informed consent was obtained in writing from each participant prior to the experiment.

B. Instrumentation

Handwriting movements and EEG signals were recorded simultaneously at sampling rates of 60 Hz and 1000 Hz, respectively. Handwriting trajectories were captured using a custom-developed application built on the PsychoPy platform, integrated with a Wacom Intuos Pro Medium tablet and Wacom Pro Pen 2 stylus featuring 8192 levels of pressure sensitivity. This application was designed to log critical events and features of each handwriting motion, including timestamps, x - and y -coordinates, rotation angles, force, and pen state codes for pen-down (contact with the surface), pen-move, and pen-up (lifting from the surface) for each digitalized point along the trajectory.

EEG signals were recorded using a 64-channel Neuroscan amplifier (Curry 9; Australia), with electrode placements following the 10–20 international system [54]. A ground electrode was referenced to maintain signal consistency.

Synchronization of handwriting trajectories with EEG signals was achieved by embedding time markers of key events within the EEG stream. Specifically, each first pen-down event of symbols written within each block on the tablet was marked for temporal alignment, as illustrated in Fig. 2(B).

C. Experimental Design

The experiment was conducted in a sound-attenuated room. Participants were seated comfortably at a desk, positioned approximately 35 cm from a tablet, which was placed in an optimal location on the desk for each individual.

The task followed an event-related design, with extended breaks provided after every 10 trials. During these breaks, participants could rest for an unlimited duration, initiating the next trial by pressing the space key. Each trial, as illustrated in Fig. 2A, began with a fixation cross displayed for 1000 ms with a random jitter of ± 500 ms. Subsequently, a letter was presented for 2000 ms, cueing the character participants were to write in the handwriting task. During this phase, participants used a stylus to write the letter slowly within a 3000 ms time frame. A 2000 ms relaxation interval followed each handwriting task.

The sequence of the 26 letters was randomized for each participant, with each letter repeated 25 times, resulting in a total of 650 trials (25×26) per participant. The entire session lasted approximately 2 hours.

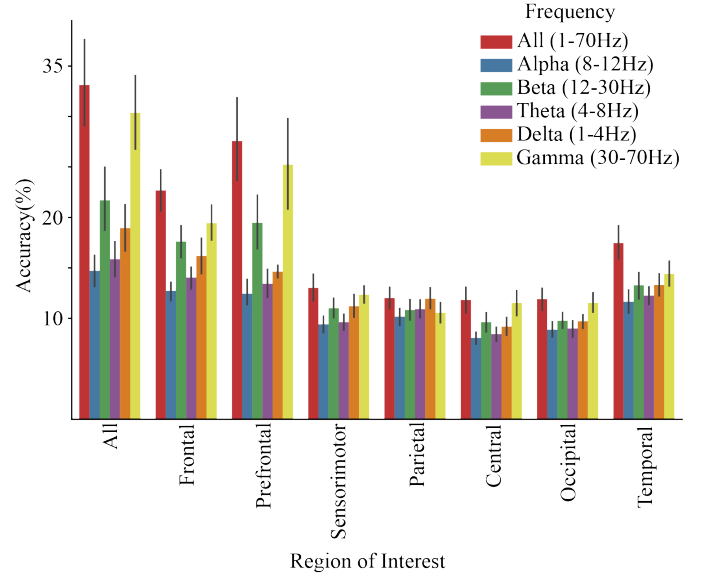


Fig. 3. Top 1 Accuracy of CNN w/ ConL Model Across Different ROIs and Frequency Bands.

D. Data Processing

a) *EEG Preprocessing*: EEG data preprocessing was performed using MNE (version 1.6.0) [55] in Python 3.10.13. The pipeline began with a bandpass filter between 1 and 70 Hz to attenuate slow drifts and high-frequency noise, followed by notch filtering at 50, 100, and 150 Hz to suppress line noise and its harmonics. EEG signals were then epoched from -1 s to 3 s relative to the first pen-down event in each trial, capturing preparatory, execution, and post-execution neural activity. Artifact handling was performed in two stages. First, automated channel-level artifact suppression was applied using

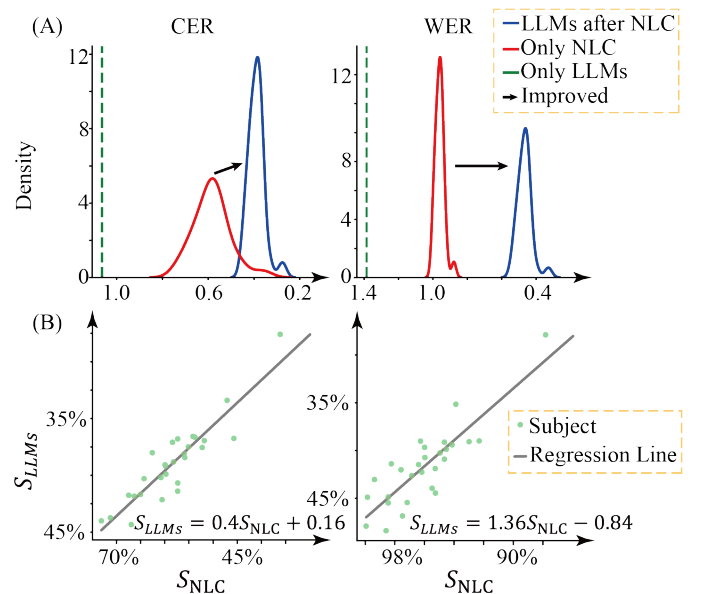


Fig. 4. (A): The Kernel Density Estimate (KDE) distributions among only neural letter classifier (NLC), only LLMs (Large Language Models, the baseline), and LLMs after NLC. (B): The linear regression between the CER and WER scores of NLC (S_{NLC}) and LLMs (S_{LLMs}).

TABLE II

PAIRED COMPARISON BETWEEN THE PROPOSED CNN-BASED MODEL AND REPRESENTATIVE BASELINES, WITH AND WITHOUT CONTRASTIVE LEARNING (CONL). ACCURACY IS REPORTED AS MEAN \pm STANDARD DEVIATION (%). STATISTICAL SIGNIFICANCE IS ASSESSED USING PAIRED T-TESTS ACROSS SUBJECT-SESSIONS, WITH * $p < 0.05$, ** $p < 0.01$, AND *** $p < 0.001$, COMPARING EACH BASELINE AGAINST THE PROPOSED CNN MODEL.

Model	Setting	Top-1	Top-3	Top-5
CNN (Proposed)	w/o ConL	27.23 \pm 12.10	51.34 \pm 14.78	65.29 \pm 12.08
	w/ ConL	33.10 \pm 11.54	57.77 \pm 12.89	71.46 \pm 11.11
LSTM	w/o ConL	18.22 \pm 3.46***	31.21 \pm 6.71***	41.66 \pm 6.42***
	w/ ConL	25.74 \pm 3.51**	37.85 \pm 4.36***	49.00 \pm 6.07***
Transformer	w/o ConL	15.54 \pm 4.40***	27.56 \pm 4.14***	36.44 \pm 4.02***
	w/ ConL	23.99 \pm 3.14***	33.22 \pm 3.00***	43.92 \pm 3.50***
EEG-Deformer	w/o ConL	17.94 \pm 4.46***	30.02 \pm 4.12***	38.82 \pm 4.04***
	w/ ConL	28.99 \pm 3.14*	38.22 \pm 3.00***	48.92 \pm 3.50***
Conformer	w/o ConL	14.59 \pm 4.57***	26.54 \pm 4.19***	35.28 \pm 3.73***
	w/ ConL	25.56 \pm 3.29**	34.37 \pm 3.58***	45.54 \pm 3.22***
EEGFormer	w/o ConL	15.21 \pm 4.97***	26.87 \pm 4.67***	35.74 \pm 3.74***
	w/ ConL	26.07 \pm 3.38**	35.16 \pm 3.19***	46.46 \pm 3.86***
TCNet	w/o ConL	16.34 \pm 4.63***	28.64 \pm 4.28***	37.46 \pm 3.96***
	w/ ConL	27.53 \pm 3.17**	36.82 \pm 3.30***	47.17 \pm 3.60***

the Autoreject framework [56] to detect and interpolate noisy channels within each epoch; no trials were discarded at this stage. This step improves data quality for subsequent analysis while preserving the full trial structure. Second, Independent Component Analysis (ICA) was applied to the epoched data after channel interpolation. ICA decomposition was performed using the FastICA algorithm implemented in MNE. Independent components were inspected following established EEG practice based on their temporal dynamics, spatial topographies, and spectral characteristics. Only clearly identifiable ocular artifacts (e.g., blink-related components and other clearly non-neural artifacts) were removed using a conservative manual procedure, with fewer than three components removed per subject. Finally, the EEG data were re-referenced to the common average, and baseline correction was applied using the pre-event interval to ensure consistency across channels.

b) *EEG Feature Extraction*: Power Spectral Density (PSD) was extracted as the primary feature for model prediction. To compute PSD, an Fast Fourier Transform (FFT) was used capturing frequencies between 1 Hz and 70 Hz, as shown in Fig. 2C. The PSD for a given signal $x(t)$ was calculated using the formula:

$$\text{PSD}(f) = \frac{1}{N} \left| \sum_{t=0}^{N-1} x(t) e^{-i2\pi ft/N} \right|^2 \quad (8)$$

where f represents the frequency, and N is the total number of time points in the signal. This approach provided a detailed frequency profile of the EEG signals, essential for downstream analyses.

c) *Trajectory Processing*: Trajectory data was processed by applying min-max normalization to the $x(t)$ and $y(t)$ coordinates, which were subsequently mapped onto a 28 x 28 pixel grid. To represent temporal progression, the intensity values along the trajectory were scaled from 50 to 255, illustrating the passage of time, as shown in Fig. 2B. This approach allowed the temporal aspects of each handwriting movement to be visually represented in the spatial grid format.

E. Stage 1: Neural Letter Classifier

1) *Model Performance Comparison*: We evaluated the performance of different neural network architectures for EEG-based letter decoding, including LSTM, transformer-based, EEG-Deformer [57], Conformer [58], EEGFormer [59], and TCNet [60], with and without ConL. The comparison focuses on Top-1, Top-3, and Top-5 classification accuracy and is summarized in Table II.

Across all evaluated models, the proposed CNN-based architecture consistently achieved the highest decoding accuracy under the current experimental setting. In particular, the CNN with ConL attained a Top-1 accuracy of 33.10% \pm 11.54%, a Top-3 accuracy of 57.77% \pm 12.89%, and a Top-5 accuracy of 71.46% \pm 11.11%, outperforming all recurrent and transformer-based baselines. Paired t-tests across subject-sessions indicate that these improvements are statistically significant in most comparisons, with multiple-comparison correction applied using the Benjamini–Hochberg procedure.

a) *Confusion matrix analysis*.: Fig. 5(A) illustrates the confusion matrix of the averaged conditional probability $P(\text{predicted} | \text{true})$ for 26 handwritten letters. Overall decoding performance varies substantially across letters. Letter *I* achieves the highest classification accuracy (33.12%), whereas letter *R* exhibits the lowest accuracy (15.00%), indicating pronounced letter-specific decoding difficulty.

Certain letters show consistently higher confusion rates. In particular, letter *E* demonstrates relatively poor performance (23.13%) and is frequently misclassified as visually or motorically similar letters, including *D*, *J*, *G*, *N*, *B*, *H*, *R*, *L*, *S*, and *X*. This widespread confusion suggests that *E* shares common stroke components and motor primitives with multiple letter classes, making it difficult to disentangle under non-invasive EEG constraints.

Fig. 5(B) further summarizes the most frequently confused letter pairs. Among them, the *M–N* pair exhibits the highest mutual confusion probability, which can be attributed to their highly similar handwriting trajectories characterized by repeated vertical strokes and comparable temporal motor patterns. Overall, these results indicate that misclassifications are highly structured rather than random, reflecting intrinsic similarities in neural and motor representations rather than decoder instability.

2) *Model Performance Across Different ROIs and Frequencies*: This section investigates the impact of different ROIs and frequency bands on the Top 1 accuracy of a CNN model augmented with ConL. The analysis focuses on the PSD extracted from specific bands and ROIs to determine their relative importance in performance metrics.

Fig. 3 illustrates the results of this comparison. Utilizing all features from all bands and ROIs yields the highest Top 1 accuracy, indicating the advantage of a comprehensive feature set. The Gamma band stands out among the frequency bands, showing the largest performance improvement, underscoring its significance in EEG-based models. Regarding the ROIs, the PFC achieves the first-highest Top 1 accuracy, followed by the whole frontal cortex. Subsequent analyses show that the temporal and sensorimotor cortices rank lower, yet they contribute to overall model accuracy.

TABLE III
MAIN DECODING RESULTS

Arch	Curriculum	BLEU (%)				ROUGE (%)				Error Rates (%)	
		1	2	3	4	1	2	L	Lsum	CER	WER
Bart-base	no	25.74	10.77	5.02	2.68	22.78	3.80	18.51	18.50	92.61	120.32
	yes	27.55	11.46	5.64	3.17	24.07	4.04	19.51	19.50	89.63	113.22
Bart-large	no	58.52	47.86	40.91	35.76	58.18	41.13	57.11	57.10	44.96	53.54
	yes	64.89	55.56	49.27	44.42	64.63	49.91	63.72	63.71	38.94	46.68

TABLE IV
ABLATION ON THE IMPACT OF SPACE SEPARATION BETWEEN WORDS DURING NEURAL SPELLING

Arch	Space	BLEU (%)				ROUGE (%)				Error Rates (%)	
		1	2	3	4	1	2	L	Lsum	CER	WER
Bart-base	no	40.14	25.47	18.24	13.97	35.24	15.12	32.00	31.97	66.46	83.10
	yes	45.46	32.01	24.92	20.37	41.15	21.96	38.30	38.27	60.89	76.22
Bart-large	no	58.52	47.86	40.91	35.76	58.18	41.13	57.11	57.10	44.96	53.54
	yes	64.89	55.56	49.27	44.42	64.63	49.91	63.72	63.71	38.94	46.68

TABLE V
ABLATION STUDY ON THE IMPACT OF LETTER CLASSIFICATION SAMPLING SPACE

Model Arch	Sample Space	BLEU (%)				ROUGE (%)				Error Rates (%)	
		1	2	3	4	1	2	L	Lsum	CER	WER
Bart-base	3	58.52	47.86	40.91	35.76	58.18	41.13	57.11	57.10	44.96	53.54
	7	51.79	39.32	31.89	26.80	49.31	30.32	47.60	47.60	53.69	64.31
	11	45.98	32.34	24.72	19.83	42.78	22.54	40.56	40.54	60.31	72.27
	15	44.62	30.68	23.06	18.29	40.97	20.65	38.63	38.61	62.08	74.78
	19	43.76	29.65	22.10	17.42	40.01	19.59	37.53	37.52	63.12	76.09
	23	43.48	29.31	21.74	17.07	39.65	19.22	37.11	37.09	63.46	76.55
	26	48.14	34.61	27.03	22.10	44.44	24.68	42.14	42.14	58.78	71.18
Bart-large	3	64.89	55.56	49.27	44.42	64.63	49.91	63.72	63.71	38.94	46.68
	7	55.22	43.30	35.94	30.73	52.74	34.52	51.12	51.13	50.72	60.95
	11	51.25	38.41	30.86	25.76	48.06	28.87	46.06	46.06	55.41	66.70
	15	49.28	36.03	28.44	23.44	45.73	26.16	43.52	43.53	57.64	69.62
	19	48.44	35.01	27.43	22.48	44.94	25.19	42.67	42.67	58.31	70.47
	23	47.94	34.37	26.78	21.85	44.30	24.48	41.98	41.97	59.13	71.60
	26	48.13	34.66	27.11	22.20	44.44	24.74	42.12	42.13	58.92	71.36

Informative EEG Feature Analysis. To explicitly investigate which EEG features are most informative for letter decoding, we analyzed decoding performance across both spectral and spatial dimensions. As shown in Fig. 3, frequency-band analysis reveals that high-frequency components, particularly the gamma band (30–70 Hz), contribute most strongly to Top-1 decoding accuracy. In contrast, lower-frequency bands (delta and theta) show relatively limited discriminative power for letter classification. Spatially, electrodes over the prefrontal and frontal cortices yield the highest decoding performance, followed by temporal and sensorimotor regions. Using all ROIs jointly achieves the best overall accuracy, indicating that neural letter representations are distributed across multiple cortical areas rather than localized to a single region. Together, these results suggest that informative features for non-invasive neural spelling are largely associated with high-frequency spectral activity in frontal–prefrontal networks associated with motor planning and language-related processing.

F. Stage 2: Curriculum-based Large Language Model

1) *Sentence Dataset:* For Stage 2 verification, we utilize the *Story-Plots-1.3k* dataset from QuasarResearch, an expansion of the *Neural-Story-v1* from NeuralNovel. This dataset is specifically designed for applications in creative text generation and narrative analysis, comprising 1,320 unique story plots. All stories are included in our testing set. The dataset is hosted on Hugging Face, available at <https://huggingface.co/datasets/QuasarResearch/story-plots-1.3k>.

2) *Sentence Decoding Performance:* Table III presents the results of sentence decoding from the encoder, utilizing the Top-k predicted distribution as input for the LLM decoder (where $k = 3$). We evaluate the decoding performance across two different model sizes of the BART model [50], namely ‘large’ and ‘base’, with the trainable parameters equal to 406M and 140M, respectively. For both model sizes, our proposed curriculum learning method significantly enhances decoding performance across all evaluated metrics. Specifically, using the pretrained BART-large model, our method achieves a BLEU-4 score of $44.42\% \pm 2.2\%$ and a ROUGE-L score of $63.71\% \pm$

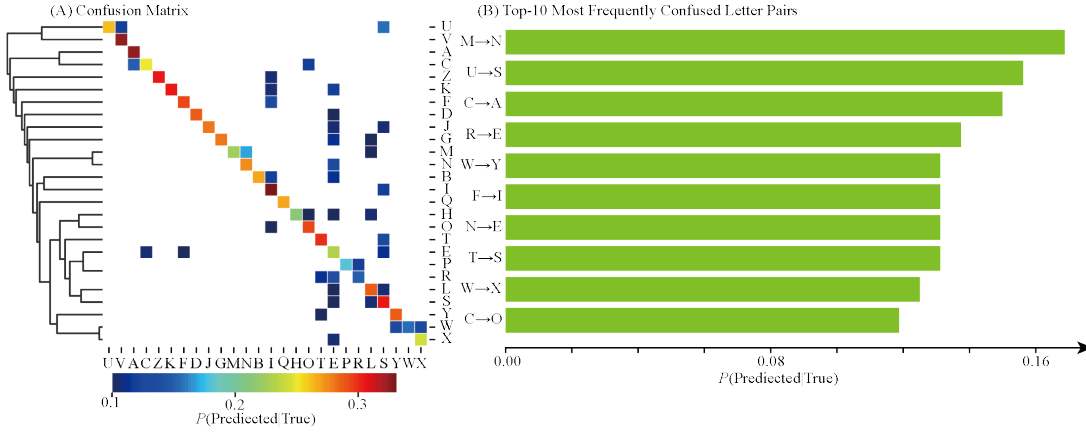


Fig. 5. (A): Confusion matrix of letter decoding performance with hierarchical clustering. The matrix shows the averaged conditional probability $P(\text{predicted} | \text{true})$ (colored $P > 0.1$) for 26 handwritten letters, reordered using hierarchical clustering based on confusion profiles. (B): Top-10 Most Frequently Confused Letter Pairs.

0.86%.

Additionally, Fig. 4(A) compares the performances among only neural letter classifier, only LLMs (baseline), and LLMs after neural letter classifier, show the LLMs can improve the performance for this spelling-based language decoding. This observation underscores the potential of LLMs to enhance the language decoding task, suggesting that improvements in letter classification directly contribute to better sentence reconstruction outcomes.

Fig. 4(B) revealing a positive linear relationship between the decoder’s performance on the sentence decoding task and the neural letter classifier’s performance. It shows that LLMs after neural letter classifier can significantly improve in word level.

3) *Visualization of Sentence Decoding Results*: For qualitative analysis, we visualize the decoding results of our method in Supplemental Table I. The input samples were taken from subject P11, who exhibited the highest letter-level classification performance in our dataset. Notably, some phrases from the initial neural decoding are already partially informative and resemble the target sentence structure. For example, the fragment ‘rn thp unltrgfving...’ bears clear similarity to the ground-truth phrase ‘in the unforgiving...’.

The LLM decoder then integrates these noisy letter-level predictions with learned word-transition statistics and linguistic constraints, enabling improved grammatical structure and word-level coherence. Importantly, the resulting sentences are not intended to be exact verbatim reconstructions of the ground truth. Instead, they represent semantically plausible and communicatively usable outputs that balance neural evidence with strong language priors.

As illustrated in Supplemental Table I, this process may introduce creative variations, particularly when the neural input is highly uncertain, reflecting a trade-off between symbol-level fidelity and language-level coherence. These qualitative results demonstrate the effectiveness of the proposed framework in refining linguistic outputs under noisy neural decoding conditions, while preserving consistency with the underlying neural evidence.

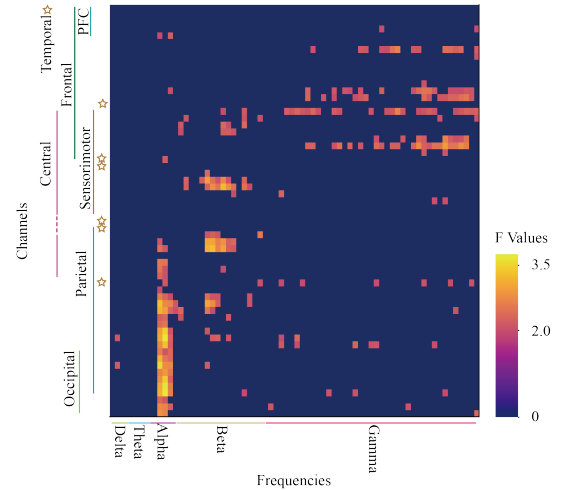


Fig. 6. Significance of EEG spectral variations across different regions and frequencies, analyzed using F-statistics ($F(25,675)$) and corrected for multiple comparisons with the FDR_BH approach (colors indicate $p < 0.05$).

G. Ablation Study

1) *Ablation on the effect of letter sampling range*: In our analysis, we observe a decline in performance across all metrics when sampling from a larger prediction range. This outcome illustrates a trade-off between letter-level prediction accuracy and input diversity. To balance these factors effectively, we opt to utilize the top-3 prediction results for each letter to sample the letters spelled by the user, as detailed in Table V. This approach optimizes our model’s accuracy while maintaining a reasonable level of diversity in the input data.

2) *Ablation on the Effect of Space Between Words During Neural Spelling*: Results are presented in Table IV. In conclusion, while incorporating spaces between words introduces an additional step for the user, it aids the model in more effectively denoising the input. However, the overall results demonstrate that our model is capable of denoising neural spelling text effectively even when spaces are not included in the input. This underscores the robustness of our approach in handling continuous streams of characters without explicit segmentation.

VI. DISCUSSION

This study presents a Curriculum-based Neural Spelling Framework comprising a Convolutional EEG Encoder and a ConL module, demonstrating the feasibility of recognizing handwritten letters using non-invasive technologies. Furthermore, the system highlights the potential for real-world applications by integrating LLMs to generate free-form sentences based on spelling-based designs.

A. Neurophysiological Correlates of Letter Recognition

From a feature perspective, our results indicate that letter decoding is strongly associated with spectral-spatial EEG patterns rather than transient time-domain signals. In particular, gamma-band activity over frontal and prefrontal regions exhibits strong discriminative power across letters. This pattern is consistent with prior literature linking gamma activity to fine motor execution and higher-order cognitive processing.

In contrast, alpha-band activity shows letter-dependent modulation mainly in parietal and central regions, which is consistent with visuomotor integration and trajectory planning during handwriting. Lower-frequency oscillations, including delta and theta bands, demonstrate increased inter-trial coherence during movement initiation but contribute less directly to class separability. These findings are consistent with a potential functional differentiation in which high-frequency spectral features are more strongly associated with letter-specific decoding performance, while low-frequency dynamics appear more related to task coordination and motor timing.

The qualitative analysis of the Event-Related Potential (ERP) results is presented in Supplemental Section II.A.

Handwriting involves complex neural coordination, engaging multiple brain regions. Fig. 8 illustrates how specific letters correspond to neural activation (A) and handwriting trajectory (B). Some letters, such as TWY, BFE, ZK, and OC, show similar patterns in both neural and trajectory patterns. The small distance of these letters, suggests a shared representation in neural processing spaces.

Significant neurophysiological variations are highlighted in Fig. 6, where the F-statistics reveal prominent differences across cerebral regions at specific frequency bands. In particular, the alpha band shows substantial activity in the occipital

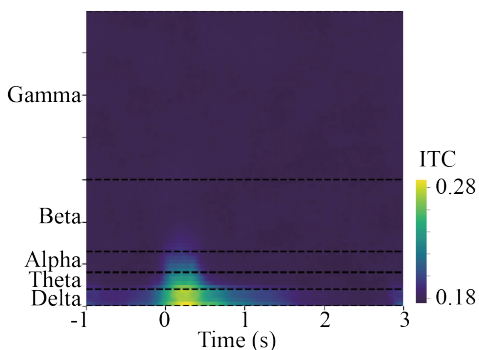


Fig. 7. Visualization of ITC across different frequencies (1Hz to 70 Hz) during handwriting tasks. The color scale indicates the level of coherence, with warmer colors representing higher coherence.

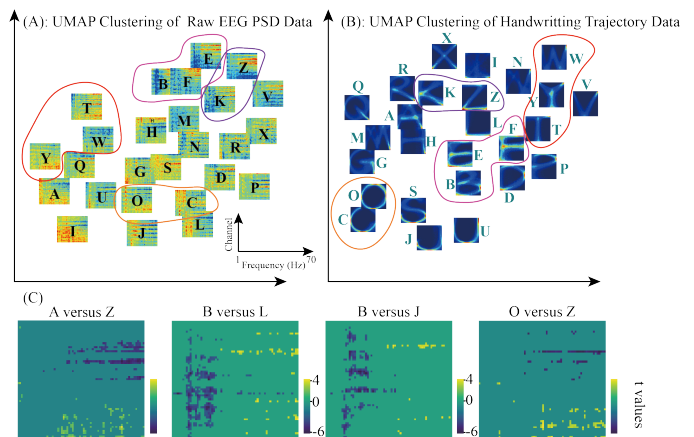


Fig. 8. UMAP visualization of letter-specific neural representations. (A): EEG PSD features with averaged baseline removed to enhance visualization clarity. (B): Handwriting trajectories showing distinct clusters for letters TWY, BFE, ZK, and OC, which suggest similar neurocognitive processing pathways and minor differences in movement patterns. (C): Significant differences between letter pairs A and Z, B and L, B and J, and O and Z, assessed via paired t-tests and corrected for multiple comparisons using the FDR_BH method (colors indicate $p < 0.05$), highlighting the neurophysiological distinctions in letter processing. UMAP embeddings were computed and visualized on a per-subject basis to account for inter-individual EEG variability.

and parietal lobes ($p < 0.05$), underscoring their roles in visual processing and spatial integration [61, 62], essential for interpreting letter shapes and trajectories.

As demonstrated in Fig. 8(C), the neural pattern differences between letters exhibit complex and diverse styles across different brain regions and frequency bands ($p < 0.05$). Specifically, the differences between letters A and Z are predominantly observed in the Gamma band within the Frontal and Parietal cortices ($p < 0.05$). In contrast, the patterns for B and L are distinctly marked by Alpha band activity in the Parietal and Central cortices ($p < 0.05$). Interestingly, the neural patterns for B and J are similar to those of B and L but feature less Gamma band activity in the Frontal cortex ($p < 0.05$). Moreover, the patterns for O and Z resemble those between A and Z, albeit with a reduced difference in Gamma activity ($p < 0.05$). These observations highlight the unique neurophysiological pathways for each letter pair, reflecting varied motor and cognitive demands, and suggesting differences in cognitive processing levels.

The frontal cortex demonstrates increased gamma-band activity, reflecting its integrative function across sensory modalities and its pivotal role in higher cognitive processes, such as memory and decision-making [63–66], which are crucial for language processing and handwriting execution.

Moreover, the prefrontal cortex (PFC) emerges as a critical node, facilitating the integration of multi-modal information and mediating complex cognitive functions including executive control and working memory [67, 68]. Similarly, temporal cortex activations are closely tied to language processing, with gamma activity playing a significant role in the neural decoding of language elements [6, 8].

Additionally, the sensorimotor cortex’s involvement aligns with its role in governing motor control and sensory processing, fundamental to handwriting [69]. The broad gamma activity

across these regions suggests a high-level synchronization of cortical activity, facilitating coherent cognitive representations necessary for complex tasks like letter recognition and differentiation [70–72].

This study underscores the nuanced interplay of multiple brain regions during letter recognition and handwriting, paralleling findings from related fMRI studies [73]. The identified patterns across the frontal, parietal, and temporal cortices substantiate their critical roles in the cognitive and perceptual foundations of language and handwriting tasks. Utilizing all ROIs and frequency bands yields the best performance, as demonstrated in Fig. 3.

We emphasize that all neurophysiological interpretations are based on correlational analyses of sensor-level EEG signals. Accordingly, observed spectral and spatial differences are interpreted as task-dependent neural associations rather than direct evidence of causal mechanisms or localized neural representations.

B. Inter-Trial Coherence in Delta Band During Handwriting Tasks

Inter-Trial Coherence (ITC) measures phase synchronization across EEG trials, providing insights into consistent neural responses and cortical synchrony during event-related cognitive tasks [74]

$$ITC(f) = \left| \frac{1}{N} \sum_{k=1}^N e^{i\phi_k(f)} \right| \quad (9)$$

where N is the number of trials, f represents the frequency, and $\phi_k(f)$ is the instantaneous phase of the k -th trial at frequency f .

Our analysis, during handwriting tasks, particularly underscores the Delta frequency band, which exhibits significant coherence during the initial phase of action execution (0 to 1 second), as depicted in Fig. 7. This heightened coherence suggests a robust engagement of neural circuits associated with low-frequency oscillations, crucial for the timing and coordination of motor movements.

Studies have indicated the involvement of Delta and Theta bands in motor tasks and cognitive processing [75]. For instance, increased ITC in these bands has been associated with task switching and inhibitory control in BCI paradigms [76]. Similar patterns of coherence in Delta-Theta ranges have been observed during motor performance improvements in stroke rehabilitation, reflecting neural reorganization and recovery [77]. In addition, heightened Theta synchronisation has also been shown to correlate with navigation workload during physical navigation, supporting the role of low-frequency oscillations in coordinating cognitive–motor demands in ecologically valid settings [78, 79]. The periodic auditory stimulation research shows a synchronization peak at 2 Hz in the Delta band, linking sensory–motor time coupling, which may parallel the neural dynamics observed during the rhythmic movements in handwriting [80].

Moreover, the Alpha band, while showing lower coherence compared to the Delta band during the initial phase of handwriting, plays a significant role in broader cognitive

and motor control contexts. Increased Alpha ITC has been associated with enhanced visuomotor performance and is particularly evident in tasks requiring visual coordination, such as visuomotor tracking [81]. Furthermore, variability in Alpha ITC has been linked to cognitive control efficiency within the frontoparietal network [82], an aspect crucial for complex task execution.

This differential engagement of frequency bands underscores the complexity of brain dynamics during fine motor tasks such as handwriting. While Delta, Theta, and Alpha oscillations may not yield the greatest contributions in NLC applications, their primary roles in initiating and coordinating motor output, coupled with their subsequent involvement in cognitive processing, illustrate a layered neural architecture that supports both the execution and cognitive integration of handwriting tasks. Although these bands do not dominate the neural decoding efforts, their influence is nonetheless crucial for the holistic understanding of motor control mechanisms.

VII. CONCLUSIONS

This study introduces a CNS that leverages the advanced capabilities of GenAI to enhance spell-based neural language decoding tasks. Our approach is distinct in integrating a CNN with a curriculum-driven LLM, promoting an innovative hybrid method in the domain of BCIs. The framework’s effectiveness is demonstrated through its application to EEG-based handwriting of all 26 letters, a novel endeavor in the field. The CNS framework notably achieves exemplary top-k accuracy across all subjects, underscoring the robustness of the EEG encoding model. Furthermore, our curriculum supervised fine-tuning method significantly advances the state of the art by enabling the LLM to effectively learn subject-specific letter transition patterns. This methodological innovation not only enhances sentence synthesis quality but also establishes a system-level strategy for compensating low-SNR neural decoding through language-level error correction. This work addresses a translational feasibility question by demonstrating how full-alphabet neural spelling and curriculum-adapted generative language models can be integrated within non-invasive EEG constraints. By seamlessly merging non-invasive EEG with GenAI, this study advances the methodological foundation of neural spelling systems and sets the stage for future investigations into more constrained paradigms, including online operation and reduced-movement or imagery-based settings.

VIII. LIMITATIONS

The present study has several limitations. First, all experiments are conducted in an offline decoding setting, and system performance under real-time operation remains to be validated. Second, the current framework primarily relies on within-subject training, which limits cross-subject generalizability and scalability. Third, the dataset size per subject is relatively limited, constraining the training of larger or more expressive neural encoders.

In addition, the proposed neural handwriting paradigm involves overt motor execution, which restricts direct applicability

to individuals with severe motor impairments. We therefore position this paradigm as a high-SNR setting for studying full-alphabet neural spelling and language-level correction.

IX. FUTURE WORK

Future work will extend the proposed framework toward realistic online BCI deployment. Low-latency neural decoding can be achieved using lightweight convolutional models, while language-level correction can operate asynchronously, enabling responsive closed-loop interaction. Future studies will focus on end-to-end online validation, latency analysis, and long-term stability under continuous use, as well as extending the paradigm to reduced-movement or imagery-based settings to improve accessibility. In terms of scalability, future work will prioritize reduced-calibration and few-shot adaptation strategies rather than fully subject-independent decoding, which remains challenging for non-invasive EEG due to substantial inter-subject variability. Future work will also investigate constrained and confidence-aware generative decoding strategies to better balance expressive language reconstruction with reliability and user intent preservation in neural spelling systems. Future work will explicitly address safety and hallucination risks in language-level decoding by incorporating confidence-aware constraints, task-specific vocabularies, and optional human-in-the-loop verification to ensure reliable and intent-preserving communication in clinical settings. Finally, future work will systematically examine behavioral and task-related factors underlying inter-subject variability, including handwriting kinematics (e.g., speed and trajectory complexity) and effective trial counts after artifact rejection, to better contextualize individual differences in decoding performance.

REFERENCES

- [1] N. Guo *et al.*, “Ssvep-based brain computer interface controlled soft robotic glove for post-stroke hand function rehabilitation,” *IEEE Transactions on Neural Systems and Rehabilitation Engineering*, vol. 30, pp. 1737–1744, 2022.
- [2] X. Chen *et al.*, “Combination of augmented reality based brain-computer interface and computer vision for high-level control of a robotic arm,” *IEEE Transactions on Neural Systems and Rehabilitation Engineering*, vol. 28, no. 12, pp. 3140–3147, 2020.
- [3] B. Cao *et al.*, “Building eeg-based cad object selection intention discrimination model using convolutional neural network (cnn),” *Advanced Engineering Informatics*, vol. 52, p. 101548, 2022.
- [4] M.-D. Nguyen *et al.*, “Edge ai–brain-computer interfaces system: A survey,” *IEEE Transactions on Neural Systems and Rehabilitation Engineering*, 2025.
- [5] C.-T. Lin and T.-T. N. Do, “Direct-sense brain–computer interfaces and wearable computers,” *IEEE Transactions on Systems, Man, and Cybernetics: Systems*, vol. 51, no. 1, pp. 298–312, 2020.
- [6] G. K. Anumanchipalli *et al.*, “Speech synthesis from neural decoding of spoken sentences,” *Nature*, vol. 568, no. 7753, pp. 493–498, 2019.
- [7] M. Angrick *et al.*, “Real-time synthesis of imagined speech processes from minimally invasive recordings of neural activity,” *Communications Biology*, vol. 4, no. 1, p. 1055, 2021.
- [8] F. R. Willett *et al.*, “A high-performance speech neuroprosthesis,” *Nature*, vol. 620, no. 7976, pp. 1031–1036, 2023.
- [9] J. Tang *et al.*, “Semantic reconstruction of continuous language from non-invasive brain recordings,” *Nature Neuroscience*, vol. 26, no. 5, pp. 858–866, 2023.
- [10] N. Hesam-Shariati *et al.*, “Evaluation of the effectiveness of a novel brain-computer interface neuromodulatory intervention to relieve neuropathic pain following spinal cord injury: protocol for a single-case experimental design with multiple baselines,” *JMIR Research Protocols*, vol. 9, no. 9, p. e20979, 2020.
- [11] A. Défossez *et al.*, “Decoding speech perception from non-invasive brain recordings,” *Nature Machine Intelligence*, vol. 5, no. 10, pp. 1097–1107, 2023.
- [12] Z. Wang and H. Ji, “Open Vocabulary Electroencephalography-to-Text Decoding and Zero-Shot Sentiment Classification,” *Proceedings of the AAAI Conference on Artificial Intelligence*, vol. 36, no. 5, pp. 5350–5358, 2022.
- [13] S. Metzger *et al.*, “Generalizable spelling using a speech neuroprosthesis in an individual with severe limb and vocal paralysis,” *Nature Communications*, vol. 13, 11 2022.
- [14] X. Chen *et al.*, “High-speed spelling with a noninvasive brain–computer interface,” *Proceedings of the national academy of sciences*, vol. 112, no. 44, pp. E6058–E6067, 2015.
- [15] F. R. Willett *et al.*, “High-performance brain-to-text communication via handwriting,” *Nature*, vol. 593, no. 7858, pp. 249–254, 2021.
- [16] C. Zhang *et al.*, “Efficient eye typing with 9-direction gaze estimation,” *Multimedia Tools and Applications*, vol. 77, pp. 19 679–19 696, 2018.
- [17] C.-H. H. Yang *et al.*, “Large language model based generative error correction: A challenge and baselines for speech recognition, speaker tagging, and emotion recognition,” in *2024 IEEE Spoken Language Technology Workshop (SLT)*. IEEE, 2024, pp. 371–378.
- [18] C. Feng *et al.*, “Acoustic inspired brain-to-sentence decoder for logosyllabic language,” *bioRxiv*, 2024.
- [19] A. Tripathi *et al.*, “NeuroAiR: Deep Learning Framework for Airwriting Recognition From Scalp-Recorded Neural Signals,” *IEEE Transactions on Instrumentation and Measurement*, vol. 73, pp. 1–13, 2024.
- [20] L. Pei and G. Ouyang, “Online recognition of handwritten characters from scalp-recorded brain activities during handwriting,” *Journal of Neural Engineering*, vol. 18, no. 4, p. 046070, 2021.
- [21] M. A. Fodor *et al.*, “Evaluation of efficient and performance-retaining cvep-bci class augmentation,” in *2025 13th International Conference on Brain-Computer Interface (BCI)*, 2025, pp. 1–6.
- [22] L. A. Farwell and E. Donchin, “Talking off the top of your head: toward a mental prosthesis utilizing event-related brain potentials,” *Electroencephalography and Clinical Neurophysiology*, vol. 70, no. 6, pp. 510–523, Dec. 1988.
- [23] J. Hong *et al.*, “ChatBCI-4-ALS: A high-performance, LLM-driven, intent-based BCI communication system for individuals with ALS,” in *Proceedings of the Annual International Conference of the IEEE Engineering in Medicine and Biology Society (EMBS)*, Jul. 2025, pp. 1–6.
- [24] S. Luo *et al.*, “Stable Decoding from a Speech BCI Enables Control for an Individual with ALS without Recalibration for 3 Months,” *Advanced Science*, p. 2304853, 2023.
- [25] S. Zou *et al.*, “Cross-Modal Cloze Task: A New Task to Brain-to-Word Decoding,” in *Findings of the Association for Computational Linguistics: ACL 2022*. Association for Computational Linguistics, 2022, pp. 648–657.
- [26] Y. Liu *et al.*, “Decoding and synthesizing tonal language speech from brain activity,” *Science Advances*, vol. 9, no. 23, p. eadh0478, 2023.
- [27] M. J. Vansteensel *et al.*, “Fully implanted brain–computer interface in a locked-in patient with als,” *New England Journal of Medicine*, vol. 375, no. 21, pp. 2060–2066, 2016.
- [28] S. L. Metzger *et al.*, *Highly Generalizable Spelling Using a Silent-Speech BCI in a Person with Severe Anarthria*. Cham: Springer Nature Switzerland, 2024, pp. 21–28.
- [29] A. Kapur *et al.*, “Non-Invasive Silent Speech Recognition in Multiple Sclerosis with Dysphonia,” in *Proceedings of the Ma-*

- chine Learning for Health NeurIPS Workshop, ser. Proceedings of Machine Learning Research, A. V. Dalca *et al.*, Eds., vol. 116. PMLR, 13 Dec 2020, pp. 25–38.
- [30] G. Krishna *et al.*, “Speech recognition with no speech or with noisy speech,” in *ICASSP 2019-2019 IEEE International Conference on Acoustics, Speech and Signal Processing (ICASSP)*. IEEE, 2019, pp. 1090–1094.
- [31] D. Vorontsova *et al.*, “Silent eeg-speech recognition using convolutional and recurrent neural network with 85”
- [32] P. Kumar *et al.*, “Fusion of neuro-signals and dynamic signatures for person authentication,” *Sensors*, vol. 19, no. 21, p. 4641, 2019.
- [33] R. Saini, “Don’t just sign use brain too: A novel multimodal approach for user identification and verification,” *Information Sciences*, 2018.
- [34] B. Min *et al.*, “Recent advances in natural language processing via large pre-trained language models: A survey,” *ACM Computing Surveys*, vol. 56, pp. 1–40, 2021.
- [35] H. Wang *et al.*, “Pre-trained language models and their applications,” *Engineering*, 2022.
- [36] J. Devlin *et al.*, “Bert: Pre-training of deep bidirectional transformers for language understanding,” in *North American Chapter of the Association for Computational Linguistics*, 2019.
- [37] A. Radford and K. Narasimhan, “Improving language understanding by generative pre-training,” in *Preprint*, 2018.
- [38] T. B. Brown *et al.* Language Models are Few-Shot Learners.
- [39] L. Wang *et al.*, “Document-level machine translation with large language models,” in *Proceedings of the 2023 Conference on Empirical Methods in Natural Language Processing*, H. Bouamor *et al.*, Eds. Singapore: Association for Computational Linguistics, Dec. 2023, pp. 16 646–16 661.
- [40] W. Zhu *et al.*, “Multilingual Machine Translation with Large Language Models: Empirical Results and Analysis,” in *Findings of the Association for Computational Linguistics: NAACL 2024*. Association for Computational Linguistics, 2024, pp. 2765–2781.
- [41] Y. Li *et al.* Large Language Model Should Understand Pinyin for Chinese ASR Error Correction.
- [42] Y. Fan *et al.*, “Grammargpt: Exploring open-source llms for native chinese grammatical error correction with supervised fine-tuning,” in *Natural Language Processing and Chinese Computing*, F. Liu *et al.*, Eds. Cham: Springer Nature Switzerland, 2023, pp. 69–80.
- [43] L. Shu *et al.*, “RewriteLM: An Instruction-Tuned Large Language Model for Text Rewriting,” *Proceedings of the AAAI Conference on Artificial Intelligence*, vol. 38, no. 17, pp. 18 970–18 980, 2024-03-24.
- [44] Y. Chu *et al.*, “Qwen-audio: Advancing universal audio understanding via unified large-scale audio-language models,” *ArXiv*, vol. abs/2311.07919, 2023.
- [45] Y. Li *et al.*, “Using Large Language Model for End-to-End Chinese ASR and NER,” in *Interspeech 2024*. ISCA, 2024, pp. 822–826.
- [46] C.-H. H. Yang *et al.*, “Generative speech recognition error correction with large language models and task-activating prompting,” *2023 IEEE Automatic Speech Recognition and Understanding Workshop (ASRU)*, pp. 1–8, 2023.
- [47] R. Ma *et al.*, “Can generative large language models perform asr error correction?” *ArXiv*, vol. abs/2307.04172, 2023.
- [48] OpenAI, “Gpt-4 technical report,” in *OpenAI*, 2023.
- [49] A. Zeng *et al.*, “GLM-130b: An open bilingual pre-trained model,” in *The Eleventh International Conference on Learning Representations*, 2023.
- [50] M. Lewis, “Bart: Denoising sequence-to-sequence pre-training for natural language generation, translation, and comprehension,” *arXiv preprint arXiv:1910.13461*, 2019.
- [51] C. Raffel *et al.*, “Exploring the limits of transfer learning with a unified text-to-text transformer,” *J. Mach. Learn. Res.*, vol. 21, no. 1, Jan. 2020.
- [52] Y. Qiu and Y. Jin, “Chatgpt and finetuned bert: A comparative study for developing intelligent design support systems,” *Intelligent Systems with Applications*, vol. 21, p. 200308, 2024.
- [53] K. He *et al.*, “Deep residual learning for image recognition,” in *2016 IEEE Conference on Computer Vision and Pattern Recognition (CVPR)*, 2016, pp. 770–778.
- [54] H. H. Jasper, “The ten-twenty electrode system of the international federation,” *Electroencephalography and Clinical Neurophysiology*, vol. 10, pp. 371–375, 1958.
- [55] A. Gramfort *et al.*, “Meg and eeg data analysis with mne-python,” *Frontiers in Neuroscience*, vol. 7, 2013.
- [56] M. Jas *et al.*, “Autoreject: Automated artifact rejection for meg and eeg data,” *NeuroImage*, vol. 159, pp. 417–429, 2017.
- [57] Y. Ding *et al.*, “Eeg-deformer: A dense convolutional transformer for brain-computer interfaces,” *IEEE Journal of Biomedical and Health Informatics*, vol. 29, no. 3, pp. 1909–1918, 2025.
- [58] Y. Song *et al.*, “Eeg conformer: Convolutional transformer for eeg decoding and visualization,” *IEEE Transactions on Neural Systems and Rehabilitation Engineering*, vol. 31, pp. 710–719, 2023.
- [59] Z. Wan *et al.*, “Eegformer: A transformer-based brain activity classification method using eeg signal,” *Frontiers in Neuroscience*, vol. 17, 2023.
- [60] T. M. Ingolfsson *et al.*, “Eeg-tcnnet: An accurate temporal convolutional network for embedded motor-imagery brain-machine interfaces,” 2020.
- [61] S. Galetta, “Occipital lobe,” in *Encyclopedia of the Neurological Sciences (Second Edition)*, M. J. Aminoff and R. B. Daroff, Eds. Oxford: Academic Press, 2014, pp. 626–632.
- [62] J. Gottlieb and L. H. Snyder, “Spatial and non-spatial functions of the parietal cortex,” *Current Opinion in Neurobiology*, vol. 20, pp. 731–740, 2010.
- [63] N. Kanayama *et al.*, “Crossmodal effect with rubber hand illusion and gamma-band activity,” *Psychophysiology*, vol. 44 3, pp. 392–402, 2007.
- [64] T. R. Schneider *et al.*, “Enhanced eeg gamma-band activity reflects multisensory semantic matching in visual-to-auditory object priming,” *NeuroImage*, vol. 42, pp. 1244–1254, 2008.
- [65] F. Roux *et al.*, “Gamma-band activity in human prefrontal cortex codes for the number of relevant items maintained in working memory,” *Journal of Neuroscience*, vol. 32, no. 36, pp. 12 411–12 420, 2012.
- [66] K. Cho *et al.*, “Gamma rhythms link prefrontal interneuron dysfunction with cognitive inflexibility in dlx5/6+/- mice,” *Neuron*, vol. 85, no. 6, pp. 1332–1343, 2015.
- [67] V. Menon and M. D’Esposito, “The role of pfc networks in cognitive control and executive function,” *Neuropsychopharmacology*, vol. 47, pp. 1–14, 08 2021.
- [68] L. Carelli *et al.*, “Brain-computer interface for clinical purposes: Cognitive assessment and rehabilitation,” *BioMed Research International*, vol. 2017, no. 1, p. 1695290, 2017.
- [69] B. J. Sessle, “Chapter 1 - the biological basis of a functional occlusion: The neural framework,” in *Functional Occlusion in Restorative Dentistry and Prosthodontics*, I. Klineberg and S. E. Eckert, Eds. Mosby, 2016, pp. 3–22.
- [70] J. Misselhorn *et al.*, “Synchronization of sensory gamma oscillations promotes multisensory communication,” *eNeuro*, vol. 6, no. 5, pp. ENEURO.0101–19.2019, 2019, 31 Oct. 2019.
- [71] S. M. Doesburg *et al.*, “Large-scale gamma-band phase synchronization and selective attention,” *Cerebral cortex*, vol. 18 2, pp. 386–96, 2008.
- [72] C. A. Bosman *et al.*, “Functions of gamma-band synchronization in cognition: from single circuits to functional diversity across cortical and subcortical systems,” *European Journal of Neuroscience*, vol. 39, 2014.
- [73] A. G. Huth *et al.*, “Natural speech reveals the semantic maps that tile human cerebral cortex,” *Nature*, vol. 532, pp. 453 – 458, 2016.
- [74] S. Makeig *et al.*, “Mining event-related brain dynamics,” *Trends in cognitive sciences*, vol. 8, no. 5, pp. 204–210, 2004.

- [75] C.-T. Lin *et al.*, “Effects of multisensory distractor interference on attentional driving,” *IEEE Transactions on intelligent transportation systems*, vol. 23, no. 8, pp. 10 395–10 403, 2022.
- [76] J. A. Barrios *et al.*, “Delta-theta intertrial phase coherence increases during task switching in a bci paradigm,” in *International Work-Conference on the Interplay Between Natural and Artificial Computation*, 2017.
- [77] A. Gyulai *et al.*, “Inter trial coherence of low-frequency oscillations in the course of stroke recovery,” *Clinical Neurophysiology*, vol. 132, pp. 2447–2455, 2021.
- [78] T.-T. N. Do *et al.*, “Estimating the cognitive load in physical spatial navigation,” in *2020 IEEE Symposium Series on Computational Intelligence (SSCI)*. IEEE, 2020, pp. 568–575.
- [79] ———, “Retrosplenial segregation reflects the navigation load during ambulatory movement,” *IEEE Transactions on Neural Systems and Rehabilitation Engineering*, vol. 29, pp. 488–496, 2021.
- [80] U. Will and E. Berg, “Brain wave synchronization and entrainment to periodic acoustic stimuli,” *Neuroscience Letters*, vol. 424, pp. 55–60, 2007.
- [81] A. J. Rilk *et al.*, “Alpha coherence predicts accuracy during a visuomotor tracking task,” *Neuropsychologia*, vol. 49, pp. 3704–3709, 2011.
- [82] W. Aaron *et al.*, “Variability in inter-trial coherence predicts variability in cognitive control efficiency,” *Frontiers in Human Neuroscience*, vol. 9, 2015.